Forcing of Northern Hemisphere Climate Trends

EDWIN K. SCHNEIDER

George Mason University, Fairfax, Virginia, and Center for Ocean–Land–Atmosphere Studies, Calverton, Maryland

LENNART BENGTSSON

Environmental Systems Science Centre, Reading, United Kingdom, and Max Planck Institute for Meteorology, Hamburg, Germany

ZENG-ZHEN HU

Center for Ocean–Land–Atmosphere Studies, Calverton, Maryland

(Manuscript received 18 April 2002, in final form 14 January 2003)

ABSTRACT

The impact of observed global SST trends during the second half of the twentieth century on the Northern Hemisphere extratropical winter atmospheric circulation is investigated using ensembles of simulations with the Center for Ocean–Land–Atmosphere Studies (COLA) atmospheric GCM. In contrast to some other studies, the simulated ensemble mean 500-hPa trends in the North Atlantic sector do not resemble the observed trend. However, the intraensemble variability of the trends is large, with the dominant structure of that variability resembling the Arctic Oscillation ''annular mode.'' The model results are consistent with the interpretation that the observed trend is dominated by the forced signal in the Pacific–North America sector, while over the rest of the Northern Hemisphere, and especially the North Atlantic sector, the trend is primarily interdecadal timescale internal atmospheric noise with an annular structure.

In order to diagnose the origins of the forced component of the model trend, a series of equilibrium response simulations is performed using constant-in-time SST anomalies with the structure of the trend superimposed on the annually varying climatological SST. It is found that the SST trend in the latitude belt from 20°S to 20°N is responsible for forcing much of the extratropical trend, and that the dominant tropical forcing is the SST trend in the Indian Ocean/western Pacific and eastern Pacific sectors. The idealized experiments show that the precipitation response in the Tropics is linearly related to the SST trend, and that the NH December–January–February height response to SST anomalies in various regions is quasi-linear.

Some additional analysis and interpretation is given. The extratropical response to low-latitude SST trends in the idealized experiments has characteristics reminiscent of Rossby wave trains forced by tropical deep convection. The intraensemble variability in the model's extratropical zonal mean height trend, which cannot be explained by external forcing, appears to be due to variability in the trends of midlatitude eddy stirring. The observed zonal mean trend also shows evidence of forcing by trends in the eddy stirring.

1. Introduction

The Northern Hemisphere winter atmospheric circulation has displayed noticeable trends over the past half century (Fig. 1a). Understanding the origin of these trends is important for evaluating and predicting human influence on climate (Wallace and Thompson 2002), and it is the purpose of this study to add to this understanding.

Wallace and Thompson (2002, their Fig. 1) point out an interesting resemblance between the structure of the NH December–January–February (DJF) sea level pressure (SLP) trend and that of the Arctic Oscillation (AO) ''annular mode,'' which is the primary mode of high-frequency extratropical sea level pressure variability given by empirical orthogonal function (EOF) decomposition, and which is closely related to the North Atlantic Oscillation (NAO) pattern in the Atlantic region. However, there are regions where the trend/AO resemblance is not strong, particularly the Pacific–North America (PNA) sector. Thompson et al. (2000) divide the trend into the part congruent to the AO and a residual, in order to exploit this partial resemblance. Statistical analyses of observed NH DJF AO trends (Thompson et al. 2000; Feldstein 2002) conclude that the trends are statistically significant (not explicable by internal variability), given the level of the internal atmospheric noise.

Models are not in agreement as to the mechanism for

Corresponding author address: Dr. Edwin K. Schneider, Center for Ocean–Land–Atmosphere Studies, 4041 Powder Mill Rd., Suite 302, Calverton, MD 20705-3106.
E-mail: schneide@cola.iges.org

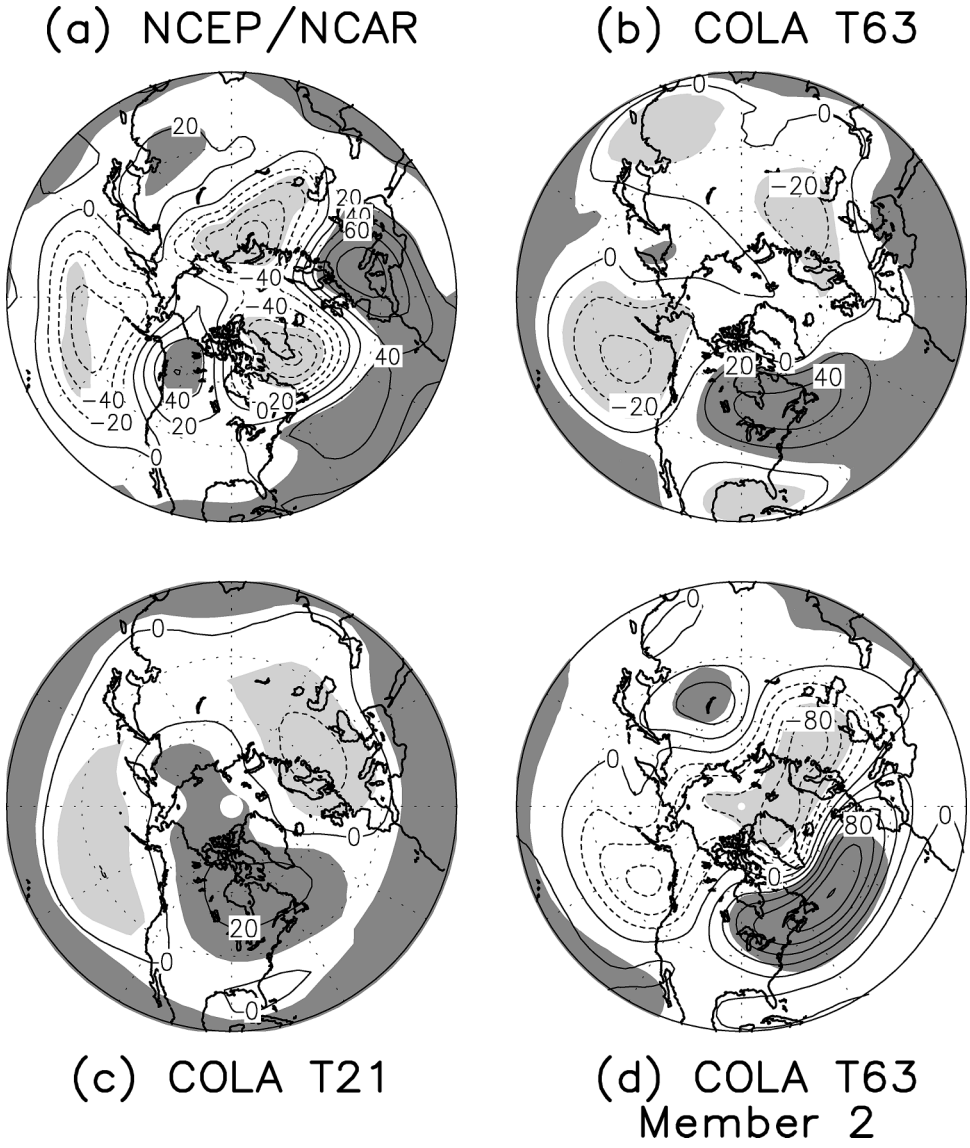

FIG. 1. Linear trend of the 500-hPa DJF geopotential height of (a) the 1948 ~ 1999 NCEP–NCAR reanalysis data, (b) trend of the mean of a 10-member ensemble of integrations with a T63 version of the COLA AGCM forced by observed 1948–99 SST, (c) as in (b) for a T21 ensemble, and (d) a particular member of the T63 ensemble. The contour interval is 20 m (50 yr)$^{-1}$. Shading indicates 95% confidence.

observed trends in the atmospheric circulation. Simulations by Shindell et al. (1999) attribute the tropospheric trends in the AO to changes in the stratospheric circulation induced by increasing greenhouse gas concentrations (GHGs). On the other hand, Fyfe et al. (1999) simulate little projection of the NAO or AO on GHG forced climate change in coupled simulations of the past and future climate until well into the twenty-first century. The study of Hoerling et al. (2001) suggests that the observed trends, including the positive trend in the NAO-like pattern in the North Atlantic, have their origin primarily in the evolution of the tropical Indian and Pacific Ocean SST.

Ensembles of simulations of the atmospheric response to the observed time evolution of SST over the past half century by Rodwell et al. (1999), using a version of the Hadley Centre GCM, and by Mehta et al. (2000), using a version of the Goddard Laboratory for Atmospheres GCM, as well as by Hoerling et al. (2001), using National Center for Atmospheric Research (NCAR) Community Climate Model (CCM3), have shown a resemblance between the simulated and observed low-pass evolution of the wintertime NAO index, including a positive trend, at least for the mid-1960s through the mid-1990s. Rodwell et al. (1999) relate this resemblance to forcing by North Atlantic SST anomalies (SSTAs) and find no evidence for tropical forcing. Hoerling et al. (2001) find the forcing from the extratropics and the

tropical Atlantic to be small and therefore attribute the resemblance in the low-frequency behavior and trend of an index closely related to the NAO to forcing by the Indo-Pacific tropical SST evolution. On the other hand, a set of simulations by Robertson et al. (2000) using a version of the University of California, Los Angeles (UCLA) GCM attributes forcing of low-frequency variability of the NAO to SST forcing in the tropical and subtropical South Atlantic. Thus, SST anomalies in the tropical Indian and Pacific Oceans, the tropical Atlantic Ocean, and the extratropical Atlantic Ocean have all been invoked to independently and exclusively explain the same atmospheric response. A complication in the interpretation of these SST forced atmospheric GCM (AGCM) experiments was pointed out by Bretherton and Battisti (2000). They infer that AGCM experiments with specified SST could be underestimating the amplitude of stationary waves forced by midlatitude SST by more than a factor of 3, arguing from the incorrect relationship between midlatitude SST and surface heat flux anomalies always produced in such AGCM experiments and by analogy with a zero-dimensional coupled atmosphere–ocean energy balance model.

Here, trends in wintertime 500-hPa Northern Hemisphere heights simulated by ensembles made with the Center for Ocean–Land–Atmosphere Studies (COLA) GCM forced by the observed SST evolution but constant-in-time GHG are examined (section 3). In contrast to the results obtained from the CCM, the ensemble mean 500-hPa trend simulated by the COLA model in the North Atlantic sector does not resemble the observed trend. However, the intraensemble variability of the trend is large, with the dominant structure of that variability resembling the Arctic Oscillation annular mode. Individual ensemble members can have much larger amplitude trends in the North Atlantic region than the ensemble mean. The results of this model are consistent with the interpretation that the observed trend is dominated by the forced signal in the Pacific–North America sector, while over the rest of the Northern Hemisphere, and especially the North Atlantic sector, the trend is primarily interdecadal timescale internal atmospheric noise.

Idealized experiments using constant-in-time SST anomalies are used to diagnose the roles of SST anomalies in the Tropics, extratropics, and the various tropical regions in producing the forced component of the trend (sections 4 and 5). These experiments address questions of attribution, linearity, and mechanism with regard to the simulated trends. Additional analysis concerns the description of wavelike characteristics of the response and the role of stirring by transient eddies in the zonal mean (section 6).

2. Model description

The experiments are simulations of the atmospheric response to specified SST, made with an AGCM with 18 sigma levels in the vertical and two horizontal resolutions, T63 and T21 ($2.0° \times 2.0°$ and $5.6° \times 5.6°$ computational grids, respectively). The AGCM is version 2 of the COLA AGCM, which is described in detail in Schneider (2002) and references therein. The T21 version is used for the idealized experiments described in section 4. The T21 ensemble (see next section) was produced in order to justify the use of results from the idealized simulations to understand the behavior of the more realistic higher-resolution model. The T21 model differs from the T63 model in that gravity wave drag is not included. Otherwise, the two model versions have identical physics.

3. Simulated trends

a. 500-hPa geopotential

1) ENSEMBLE MEAN

The trends of the DJF 500-hPa geopotential from simulations with the COLA AGCM at two horizontal resolutions (10- and 20-member ensemble at T63 and T21, respectively) and nearly identical physics forced by 1948–98 observed SST and constant CO_2 are shown in Fig. 1. The T63 ensemble was produced as part of the Climate of the Twentieth Century model intercomparison project (C20C; Folland et al. 2002), in which an SST and sea ice analysis supplied by the Hadley Centre has been used by a number of research institutions to provide surface boundary conditions for long AGCM simulations. The trend calculations use data from 1952–98 to avoid the period of spinup in the soil moisture. The trends from the two model ensembles are basically similar, although the T21 response is somewhat weaker in the Western Hemisphere (correlation between T63 and T21 is 0.66; correlations are for 20°–90°N and use cosine–latitude weighting).

The observed (Fig. 1a) and simulated (Figs. 1b,c) trends have little resemblance. Correlation between the trends for T63 and the National Centers for Environmental Prediction (NCEP)–National Center for Atmospheric Research (NCAR) reanalysis (Kalnay et al. 1996) is only 0.20, and decreases to 0.05 between T21 and NCEP–NCAR. The simulated ridge across eastern Canada in the T63 pattern (Fig. 1b) contributes to the appearance of a north–south-oriented wave train over North America, rather than the observed east–west orientation. There are, however, some areas where the simulated patterns resemble the observed trend, especially the position and amplitude of the low in the Pacific. The structure simulated at T63 of lows over the North Atlantic and northwestern Europe and a high over the Mediterranean is similar to the observed structure, although the simulated amplitudes in these regions are small compared to the observed trend, and the low over Greenland is not statistically significant at the 5% level. Compared to the T63 pattern, the low over Europe in the T21 ensemble is shifted westward, and the trend

over Greenland is weakly positive, both of which decrease the resemblance with the observed trend.

From comparison of the COLA T63 and CCM (Hoerling et al. 2001) results, it is clear that there is model dependency in the simulated ensemble mean trend pattern in the North Atlantic region, and in the amplitude of the simulated trend in the North Pacific. Each model produces a response that resembles the observed trend in some ways, but also has significant differences. The trends in the Pacific–North American region simulated by the two models have similarities in structure and amplitude, with alternating highs and lows arcing from the eastern North Pacific to the Mexico/southeastern United States region, as opposed to the observed more east–west orientation. The COLA model produces a more realistic structure in the North Pacific, since in the CCM, the low is too confined to higher latitudes. The ridge over Canada in CCM extends westward to the Pacific, and has maximum amplitude half of that in the COLA model, both of which improve the resemblance of CCM to observations. A major difference between the two models is that the pattern produced by the CCM is closer to the observed in the Mediterranean and Greenland regions. The ridge over the Mediterranean is about twice as strong in CCM as in the COLA T63. Over Greenland, the low in CCM has a maximum magnitude of about 30 m $(50\ \text{yr})^{-1}$, as compared to 10 m $(50\ \text{yr})^{-1}$ in the COLA model, and the low in CCM extends farther south, almost to Newfoundland, as compared to only the southern tip of Greenland in COLA T63.

2) INTRAENSEMBLE VARIABILITY

As noted above, there is substantial variability of the trends of the individual ensemble members about the ensemble mean trend. Figure 1d shows the trend of a single member of the T63 ensemble, which is chosen for illustration because it is the member that resembles the amplitude of the observed trend. For this particular case, the trend in the North Atlantic sector is much larger than that in the ensemble mean (Fig. 1b). The chosen trend, with high latitude decreasing trends and midlatitude increasing trends of magnitude 100 m $(50\ \text{yr})^{-1}$ extending from eastern North America across the North Atlantic and into eastern Europe, has more in common with the observed trend than the ensemble mean does, although the positions of the major features differ somewhat from the observed (correlation with observed 0.25; the simulated pattern over the Pacific–North America is shifted eastward, and the pattern over the North Atlantic is shifted northward). The ensemble member with the highest pattern correlation with the observed trend (0.43) is very similar structurally to the CCM ensemble mean trend.

Figure 2 shows some characteristics of the variability of the T63 ensemble. Results from the T21 ensemble are similar. The magnitude of the intraensemble variability is illustrated in Fig. 2a, which shows the standard deviation of the individual T63 DJF 500-mb height trends about the ensemble mean. The intraensemble variability, which can be viewed as the noise in the trend, has centers of action where the rms amplitude exceeds 30 m over the Arctic Ocean/Greenland, the North Atlantic/western Europe, and northeastern Europe. The spatial pattern associated with the first principal component from an EOF analysis of the 10 T63 DJF 500-mb height trends (ensemble mean removed) in the region 20°–90°N is shown in Fig. 2b. This pattern explains 52% of the intraensemble noise in the trend. The pattern has been scaled with the rms amplitude of its projection on the ensemble members. Some members of the ensemble (e.g., Fig. 1d) have projections of more than double this amplitude. Clearly, the intraensemble noise is sufficiently large to compete with, and in many regions dominate, the ensemble mean, or forced, component of the trend in any single realization. The structure of the intraensemble noise in the trend also resembles (correlation 0.6) the first EOF of the monthly 500-mb height in the NCEP–NCAR reanalysis (Fig. 2c), which represents the AO.

b. Precipitation

Precipitation trends from the ensembles are shown in Fig. 3. The simulated lower-latitude precipitation trends have been compared with the 1950–98 DJF trends calculated from land station data analyzed by the Climate Research Unit (CRU) of the University of East Anglia (Hulme 1994; figure not shown). The simulated and analyzed trends agree in sign over many regions, including sub-Saharan Africa, South America, North America, Indonesia, and southern Asia, but disagree over Australia. This comparison is only suggestive, since the CRU analysis has large spatial gaps with insufficient data. Comparison with the NCEP–NCAR reanalysis precipitation trends is not appropriate, since serious problems have been found by comparison of the climatology and variability of the reanalysis precipitation product with observational estimates (Trenberth and Guillemot 1998; Kinter et al. 2002).

The trends from the ensembles are similar to that simulated by Hoerling et al. (2001). The trends from both resolutions are very similar in structure and amplitude in most regions. There are common centers of increasing precipitation over the Indian Ocean, the western Pacific, and the eastern Pacific. Common areas of decreasing precipitation are found over Indonesia, the subtropical Pacific, and the equatorial western Atlantic. Precipitation also decreases over central Africa and northern South America. Increased precipitation is found over southeast Africa and southeast South America.

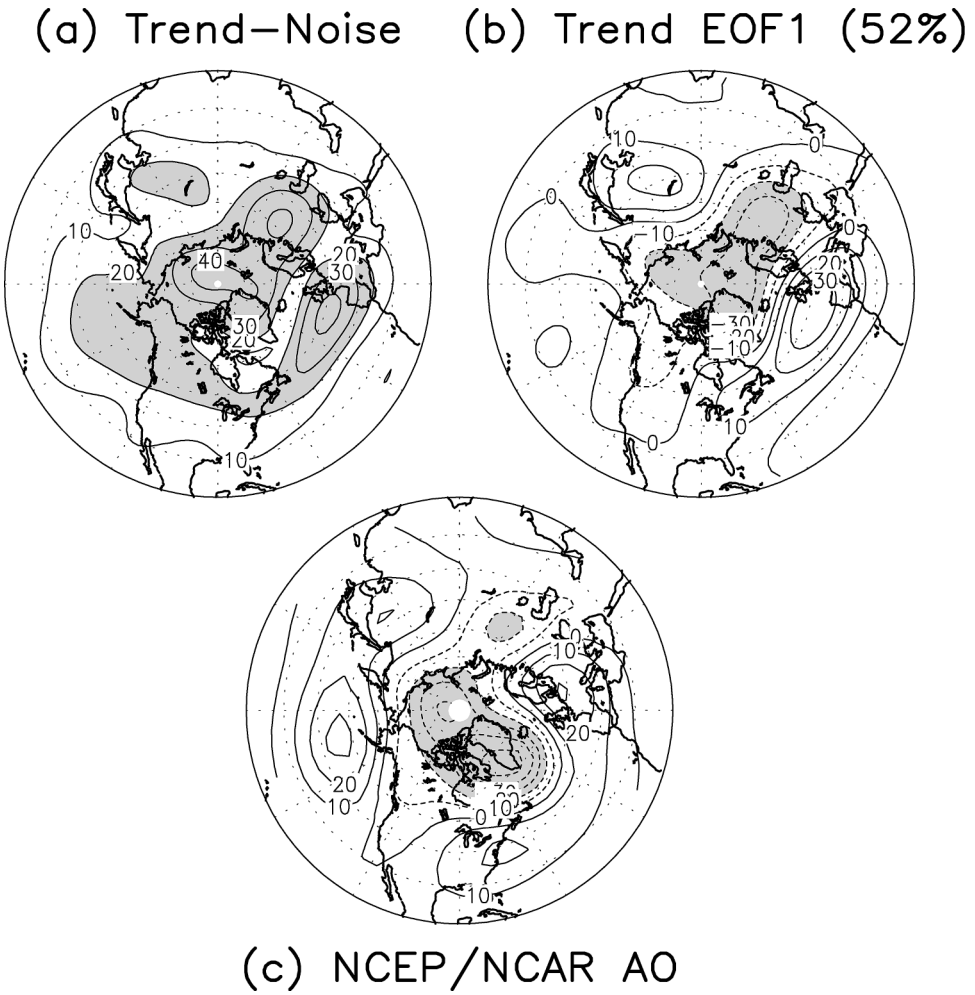

FIG. 2. (a) Rms amplitude of intraensemble variability of the NH 500-hPa DJF geopotential height trends in the T63 ensemble [units: m (50 yr)$^{-1}$]. (b) EOF1 (52%) of the trends in the T63 ensemble members (ensemble mean removed), scaled by rms amplitude of its projection [units: m (50 yr)$^{-1}$]. (c) The Arctic Oscillation in nature as represented by EOF1 (14%) of the monthly 500-hPa geopotential height anomalies, all months, trend not removed, scaled by the rms amplitude of its projection (units: m).

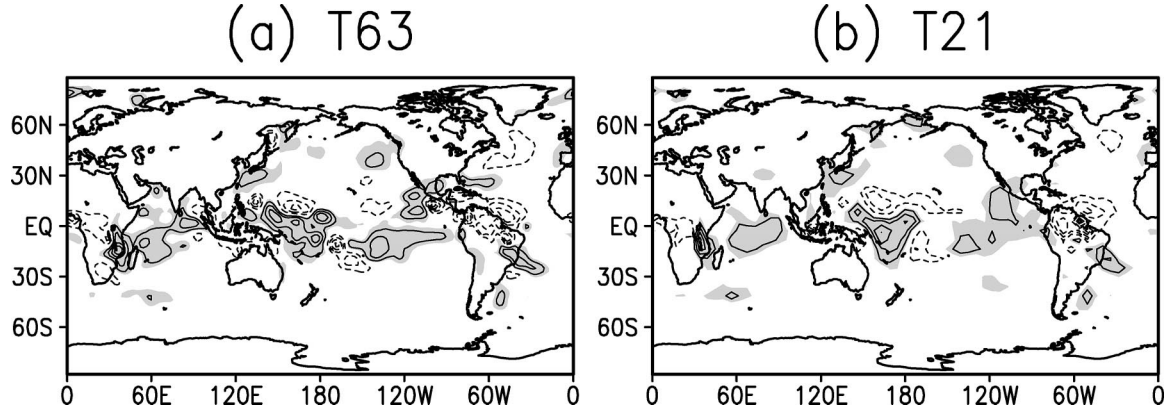

FIG. 3. Linear trend of precipitation for (a) the T63 ensemble and (b) the T21 ensemble. The contour interval is 1 mm day^{-1} (50 yr)$^{-1}$, the zero contour is not shown, and regions where the value is >0.5 mm day^{-1} (50 yr)$^{-1}$ are shaded.

TABLE 1. Description of the simulations.

Experiment	Forcing	Region applied
CONTROL	Climatological 1950–98 SST	Global
GLOBE	±Observed trend SSTA	Global
TROPICS	±Observed trend SSTA	Global Tropics 20°S~20°N, 0°~360°
EXTRATROPICS	±Observed trend SSTA	Extratropics: latitudes <20°S and >20°N
INDOPAC	±Observed trend SSTA	Tropical Indian and western Pacific Oceans 20°S~20°N, 25°E~180°
TROPATL	±Observed trend SSTA	Tropical Atlantic 20°S~20°N, 70°W~25°E
EASTPAC	±Observed trend SSTA	Tropical eastern Pacific 20°S~20°N, 70°W~180°

4. Idealized experiments: Justification and procedures

The idealized experiments are designed to attribute the trend response in the COLA model to the SST forcing in various regions, which can be done unambiguously only to the extent that the response is linear. The diagnostic experiments use the T21 coarse-resolution version of the COLA AGCM for efficiency. The trend response of this version of this model was demonstrated above to be similar to that of the T63 versions when forced by the observed SST evolution, which justifies the use of the T21 simulations for understanding the behavior of the T63 trend.

a. Experimental design

The experiments examine the global-scale influences on the atmospheric circulation of the observed trend of the SST that has occurred over the past 5 decades. One way to do this is to specify the observed evolution of SST over the time period in question as the lower boundary condition for the atmosphere, as in the simulations shown in Fig. 1. However, in order to obtain statistically robust estimates of the forced signal, especially in mid- and high latitudes, an ensemble of such simulations is required to filter out weather ''noise.'' For example, Hoerling et al. (2001) used ensembles of twelve 50-yr simulations (600 yr of model simulation) to estimate the low-frequency NAO and linear trends of the atmospheric response over the 50-yr period; Rodwell et al. (1999) and Mehta et al. (2000) used ensemble sizes of 6 and 16 in similar experiments. Here we calculate the atmospheric response to constant-in-time SST anomalies superimposed on the annually varying SST climatology. If the atmospheric response to the SST anomalies is linear, then this approach will give similar results to the ensemble approach, and will require substantially shorter simulations for robust results. Of course, the ensemble approach is much more efficient for sampling the response to the observed range of SST anomaly patterns. We use simulations of 200 yr in the idealized experiments.

The correspondence between the linear trend in the time-varying SST experiments and the size of the SSTA in the constant-in-time forced experiments is established as follows. On the timescales in question (seasonal and longer), the forced atmospheric response may be taken to be in equilibrium with the SST forcing. If these forced equilibria are linearly related to the SST anomalies, then the trend in the atmospheric response may be estimated by taking the difference between the equilibrium responses to the SST filtered to retain only the climatology plus the trend, and evaluated at the beginning and end points of the period desired. The equilibrium response is of interest no matter what the outcome; however, the results will be easiest to interpret if it is found a posteriori that the response in the idealized experiments is linear. Similar forcing has been used in GCM simulations reported by Magnusdottir and Saravanan (1999) and Magnusdottir (2001), who found the responses to constant-in-time SST anomalies derived from the zonal mean of the trend over the last century.

The SST forcings used for the experiments are derived from the observed DJF trend over the past 52 yr, with magnitude given by ½(trend × 50 yr). These forcings are added to the annually varying climatological SST from the same 52-yr period. The monthly means from the simulations interpolated to pressure levels provide the raw data for the analysis. The equilibrium responses to the specified SST anomalies are found by taking differences between the annually varying time means of the simulations.

b. Experimental procedure

Several numerical simulations with the AGCM forced by constant-in-space and constant-in-time SST anomalies were conducted in order to isolate the roles of SST forcing in the Tropics and extratropics and to examine the role of SST forcing in various tropical regions. Details of these simulations are listed in Table 1. Through linear regression, the annually varying linear trend of the monthly mean SST was first calculated at each grid point for 1948–99. The December–February SST trend is shown in Fig. 4, and is numerically twice the ''observed trend SSTA'' indicated in Table 1. The trend-derived SST anomalies are added to the 1950–98 climatological annually varying SST. The equilibrium re-

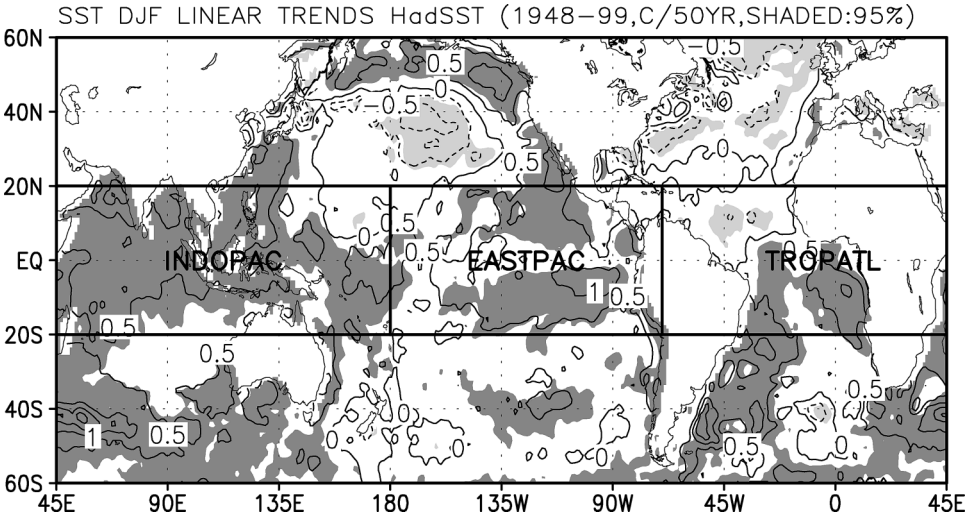

FIG. 4. SSTA used in the experiments. The SSTA (in °C) are the numerical values of the linear trends of the DJF mean SST in the 1948~1999 Hadley Centre analysis in °C (50 yr)$^{-1}$. The dark (light) shaded regions are the areas of significant positive (negative) SSTA trend at the level of 5% in the *t* test. INDOPAC, EASTPAC, and TROPATL represent the regional SSTA used in some of the experiments (see Table 1).

sponse is found for the climatological SST ± (trend SSTA), representing the end points of the trend time period. The difference between the two equilibrium responses, which will be referred to as the ''response,'' is then the estimate of the trend from the idealized simulations. By restricting the domain in which the trend forcing is taken to be nonzero, the role of the SST trend in different regions in forcing trends in the global atmospheric circulation can be estimated.

The observed SST used to derive the trends is the same Hadley Centre SST used in the simulations of the response to the observed evolution of SST. It has been our experience that the SST anomalies must be chosen carefully, since the tropical precipitation and atmospheric circulation responses are very sensitive to small SSTA changes. For example, forcing the idealized experiments by SST trends derived from the NCEP–NCAR reanalysis produces noticeably different responses than forcing by trends derived from the Hadley Centre SST.

The answer to the question of how to treat sea ice so that the climatological SST used to force the idealized experiments is consistent with that in the time varying SST experiments is not straightforward, due to the time variation of the sea ice boundary and because the model has no provision for fractional sea ice. The approach chosen here is to take the climatological SST for the idealized experiments as the annually varying time mean of the SST–sea ice surface temperature of a member of the time varying SST T21 ensemble. Another approach would be to try to define a climatological sea ice boundary. The approach taken here guarantees that the climatological ''SST'' of the time varying and idealized forcing experiments agree wherever that SST is warmer than freezing.

The SSTA is taken to be zero outside of the 20°S to 20°N band indicated in Fig. 4 in the tropical forcing simulations, which are all except CONTROL, GLOBE, and EXTRATROPICS. TROPICS uses the SSTA at all longitudes in the band, while the other three experiments, INDOPAC, EASTPAC, and TROPATL examine the effects of the SSTA restricted to the indicated longitudinal segments of the band.

5. Idealized experiments: Results

The first 3 yr of the idealized experiments are not used in order to avoid effects due to spinup of soil moisture. The response for an experiment then uses DJF means for the last 197 yr of the simulations. First, we describe the response of the Northern Hemisphere 500-hPa height. In order to aid in interpretation of these results, the precipitation and the zonal mean zonal wind are also examined.

a. Northern Hemisphere 500-hPa heights

The responses to forcing by global and regional SSTAs are shown in Fig. 5. Statistical significance calculated from the two-sided *t* test using the monthly variability of the results is indicated in the figure. Reproducibility was tested by splitting the time series into two 100 winter segments and evaluating the response for each segment. The patterns shown in Figs. 5a–f are reproducible.

1) GLOBAL SST FORCING

The DJF 500-hPa height response resulting from forcing with the global SSTA trend–anomaly in experiment

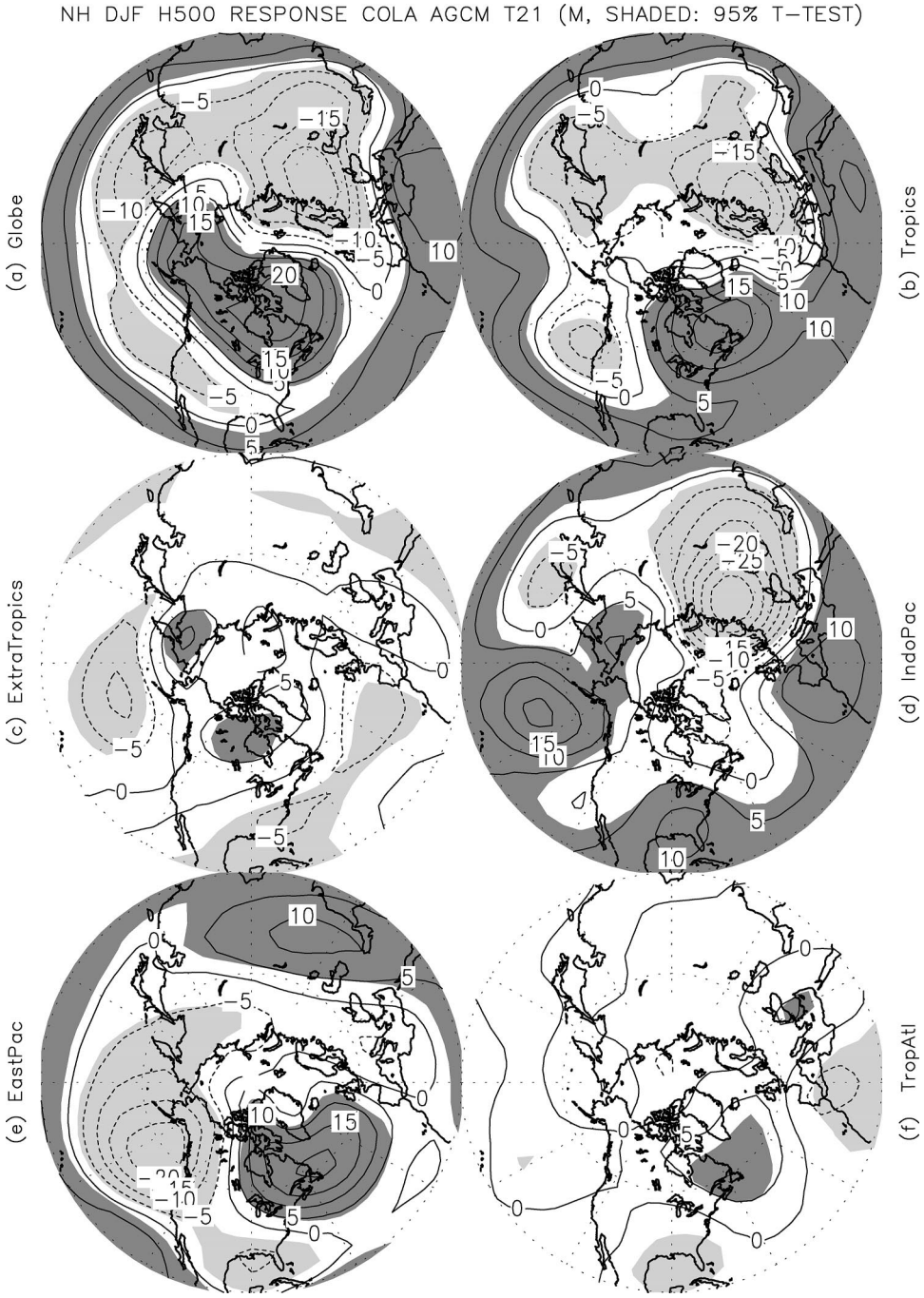

FIG. 5. Difference of DJF 500-hPa height response, positive minus negative polarity of the imposed SSTA, for experiments described in Table 1: (a) GLOBE, (b) TROPICS, (c) EXTRATROPICS, (d) INDOPAC, (e) EASTPAC, and (f) TROPATL. The contour interval is 5 m. The dark- (light-) shaded regions represent the significant positive (negative) anomalies at the level of 95% in the *t* test.

GLOBE is shown in Fig. 5a. Most of the features have a high level of statistical significance. The idealized simulation is similar to the trend found in the T21 ensemble in both structure (correlation 0.57) and magnitude (note different contour interval in Figs. 1 and 5). This similarity indicates that to some extent the idealized experiments capture the mechanisms that determine the trend of the atmospheric model ensemble mean response to the time evolving SST, and that the trend of the atmospheric response can be understood as a succession of equilibrium linear responses to the trend of the SST.

2) REGIONAL SST FORCING

The model DJF 500-hPa height response to the SSTA restricted to 20°S–20°N (TROPICS case, Fig. 5b) is clearly very similar to the response to the global SSTA (Fig. 5a), and the level of significance is high. In agreement with the result found by Hoerling et al. (2001), much of the mid- and high-latitude response to the global SSTA can be attributed to the tropical SSTA. There are noticeable differences, however. The high over Canada/eastern Siberia in GLOBE is much weaker over western Canada and extends less to the west in TROPICS, and the low-latitude ridge near the date line in TROPICS is absent in GLOBE. The response to the SSTA poleward of 20°N and 20°S (EXTRATROPICS, Fig. 5c) is relatively weak and favors higher latitudes.

The responses to SST anomalies in different regions of the Tropics are shown in Figs. 5d (INDOPAC), 5e (EASTPAC), and 5f (TROPATL). The INDOPAC response is strong over the broadest area, and has structural similarity to TROPICS, with a large low over western Europe and Asia, and a wave train–like pattern over the central Pacific and southern North America. However, the INDOPAC response is positive over the eastern Pacific/western United States, and negative over northeastern Canada, opposite in sign to TROPICS in these areas. The EASTPAC response is a strong low centered over the Gulf of Alaska and a high over northeastern North America, and also a high in south-central Asia. The response in TROPATL is weak, even compared to EXTRATROPICS. Despite the weak amplitude of the pattern, the century-to-century reproducibility and the location of the regions with a high level of statistical significance adjacent to the Atlantic gives some confidence that this pattern is good estimate of the forced response to the tropical Atlantic SSTA.

b. Tropical precipitation

The DJF tropical precipitation anomalies that correspond to the cases shown in Fig. 5 are displayed in Fig. 6. The precipitation anomalies can be interpreted as the horizontal projection of the convective heating anomalies in the various experiments. The GLOBE response (Fig. 6a) is close to the T21 ensemble precipitation trend (Fig. 3c), with differences of 1 mm day^{-1} or less. The close correspondence of the precipitation trend in the transient run ensemble mean and the response to the constant-in-time trend SSTA indicates that the model's forced tropical precipitation and circulation response to SST anomalies is very nearly linear.

Comparing Figs. 6a and 6b, it is clear that the tropical precipitation anomaly of the GLOBE experiment is captured by the TROPICS experiment. The precipitation anomalies for the longitudinally restricted SSTA experiments (Figs. 6d–f) are primarily localized in the regions of the SST anomalies. However, there are some influences of remote SST anomalies on precipitation, especially over land. Precipitation in West Africa south of the equator is sensitive to SST anomalies in both the INDOPAC and EASTPAC regions, while equatorial South American precipitation is sensitive primarily to TROPATL SST anomalies. Only GLOBE and EXTRATROPICS produce noticeable ($>$1 mm day^{-1}) precipitation anomalies in the extratropics. These precipitation anomalies are very similar in both cases, with positive anomalies in several regions in the North Pacific, in the North Atlantic near Spain, and near 40°S, and negative anomalies to the south of Greenland. Similar extratropical anomalies are also found in the ensemble mean (Fig. 3b).

c. Tropical geopotential height

The tropical 500-hPa geopotential response (not shown) contains twin highs flanking the equator at the longitudes of the important equatorial precipitation anomalies, very similar to the Gill (1980) linear-damped response to equatorial heating anomalies. In INDOPAC, the highs are centered in the Indian Ocean near 160°E; in EASTPAC, they are in the eastern Pacific near 140°W; in TROPATL they are in the central Atlantic near 30°W.

6. Interpretation

The experiments described above give estimates of both the component of the NH DJF 500-hPa geopotential height trend that is forced by the observed trend in the SST, and the magnitude and structure of the deviations from this forced trend due to ''noise'' generated by internal atmosphere/land processes, and which also may be expected to be observed in measuring the evolution of the atmosphere. The idealized experiments provide an estimate of the forced component and its origins, and are subjected to further analysis below. There is also further information that can be inferred about the origin of the noise in the trend by comparison of the reanalysis with the time-dependent experiments.

a. Forced response

The linearity of the response in the idealized experiments is examined first. Then it is shown that the extratropical height anomalies appear to be consistent with a wave propagation interpretation.

1) LINEARITY

One test of linearity is to find whether the response from one experiment can be recovered from the responses of the other experiments by linear superposition. Results from this test are shown in Fig. 7 for the 500-hPa height, where a superposition estimate of the height response for each experiment is shown, and may be compared to the actual response in the corresponding panel of Fig. 5. The pattern correlation and fractional

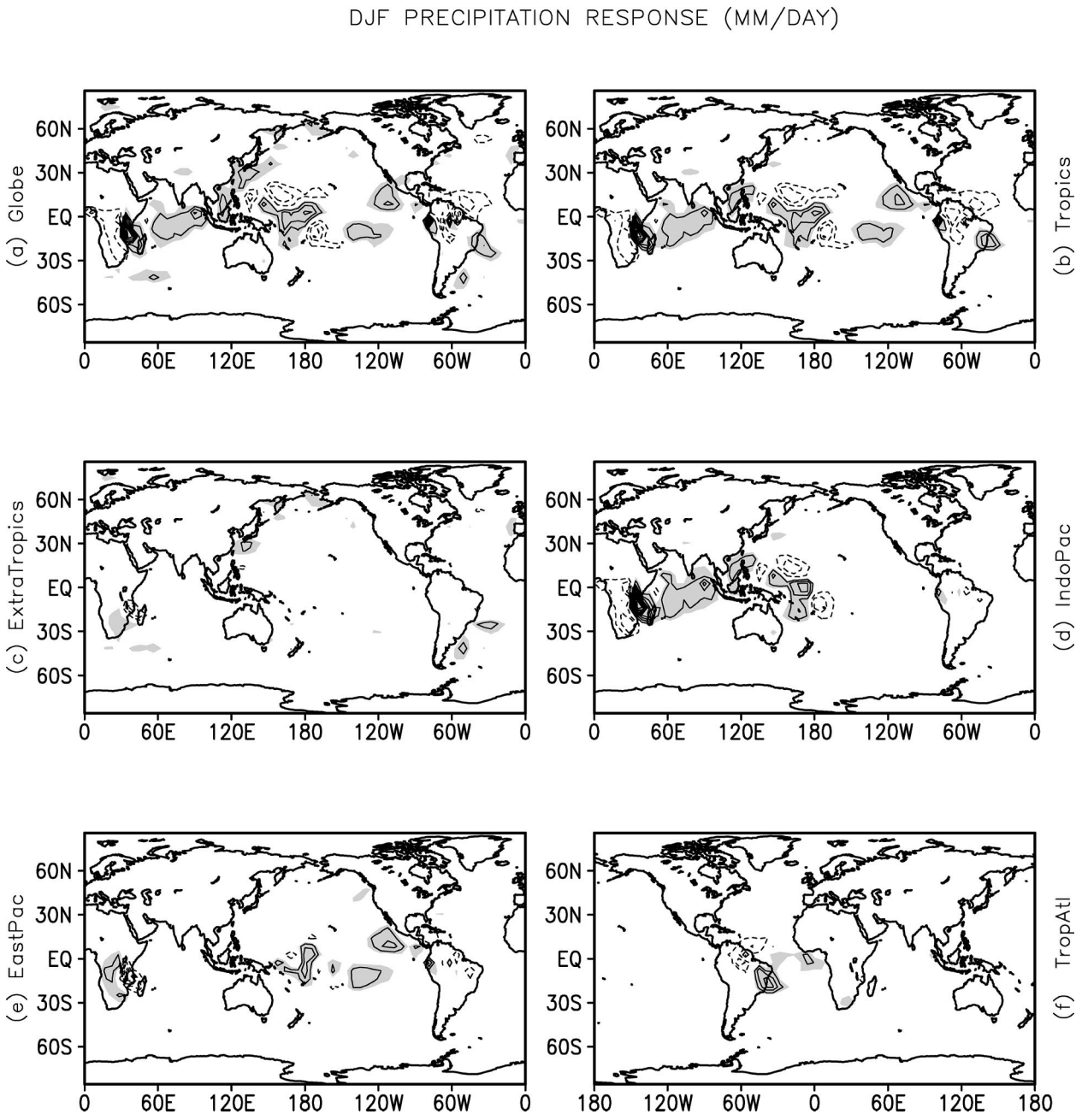

FIG. 6. Difference of DJF precipitation, positive minus negative polarity of the imposed SSTA, for experiments described in Table 1: (a) GLOBE, (b) TROPICS, (c) EXTRATROPICS, (d) INDOPAC, (e) EASTPAC, and (f) TROPATL (rotated 180° longitude from other panels). The contour interval is 1 mm day^{-1}, the zero contour is not shown, and regions where the value is >0.5 mm day^{-1} are shaded.

error with regard to the corresponding panel in Fig. 5 are given in the caption of Fig. 7. The fractional error is calculated by finding the area mean (20°–90°N) of the squared difference between the superposition and actual responses and then scaling this value by the area mean of the variance of the response. Since more than one choice is possible for each of the superpositions, a choice that better reproduces the response in Fig. 5 is shown. The GLOBE response estimated by adding the TROPICS and EXTRATROPICS responses (Fig. 7a) is very similar to the actual GLOBE response (Fig. 5a). This might be expected, given the similarity of GLOBE and TROPICS; however, adding EXTRATROPICS reduces the magnitude of the ridge near the date line found in TROPICS, and extends the high over Alaska toward Siberia, both as in GLOBE. In the representation of TROPICS (Fig. 5b) by INDOPAC + EASTPAC + TROPATL (Fig. 7b), EASTPAC and INDOPAC are out

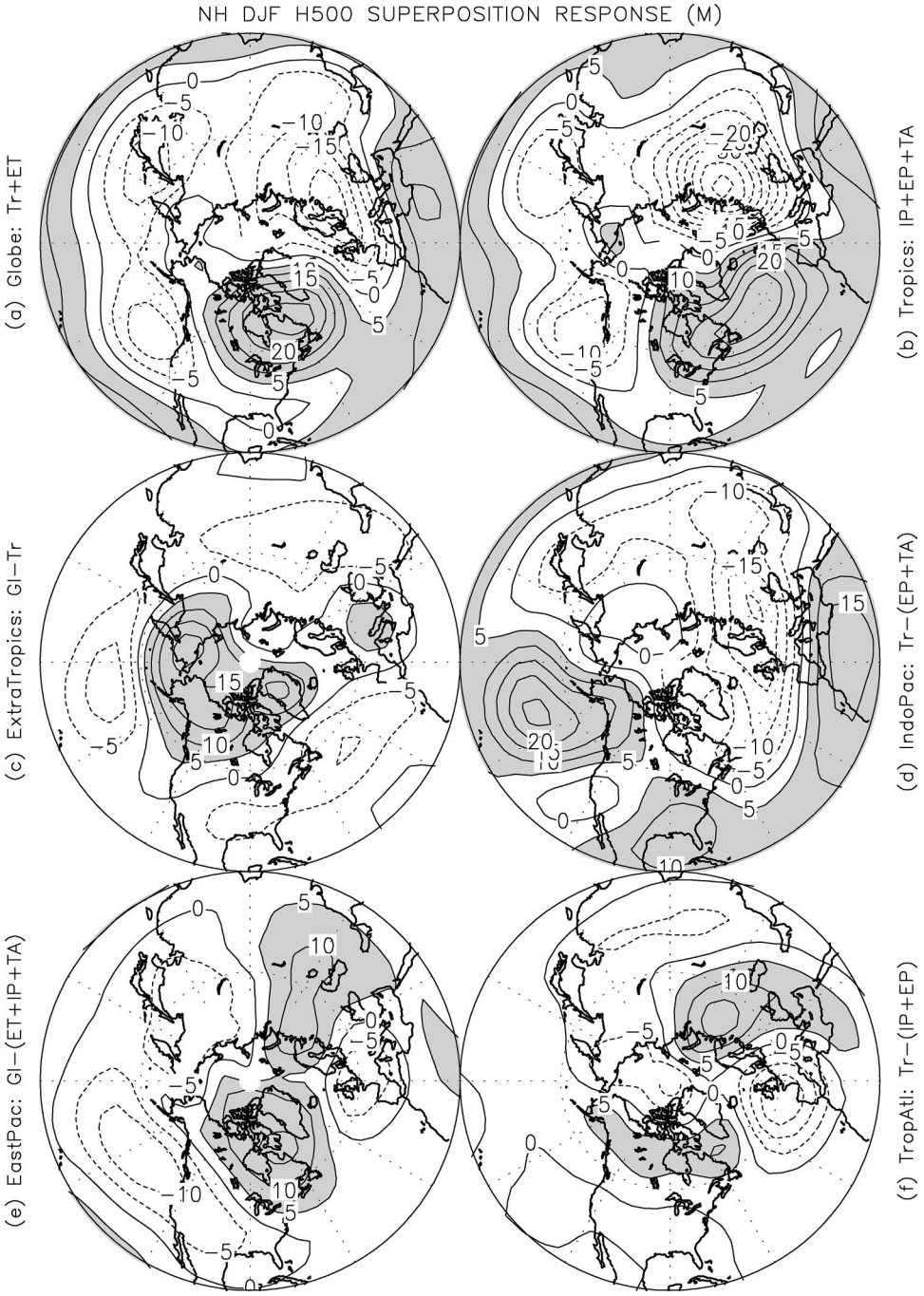

FIG. 7. Superposition of the 500-hPa responses for (a) TROPICS + EXTRATROPICS: 0.95,0.21, (b) INDOPAC + EASTPAC + TROPATI: 0.92,0.42, (c) GLOBE − TROPICS: 0.84,1.1, (d) TROPICS − (EASTPAC + TROPATL): 0.85,0.38, (e) GLOBE − (EXTRATROPICS + INDOPAC + TROPATL): 0.48,0.59, and (f) TROPICS − (INDOPAC + EASTPAC): 0.76,4.0. The contour interval is 5 m, and values >5 m are shaded. The pattern correlation *P* and fractional error *E* with respect to the corresponding panel of Fig. 5 are indicated in the legend as *P, E*.

of phase in most regions, with EASTPAC dominating in the Western Hemisphere, and INDOPAC producing the dominant response in the strong low centered over northwestern Europe. Superpositions also have some success in approximating the other responses, especially INDOPAC (Fig. 7d). Even the structures of the weaker EXTRATROPICS (Fig. 7c) and TROPATL (Fig. 7f) patterns are well correlated with the corresponding patterns in Fig. 5, although there are large errors in the amplitudes of these weaker patterns. Superposition is very

successful in reconstituting the precipitation responses. There is little point in showing a figure of the reconstituted precipitation responses, since these are nearly identical to those from the original experiments.

Another test for linearity is to examine whether the height and precipitation responses to SST anomalies of opposite sign are antisymmetric about the climate of the zero SST anomaly CONTROL experiment. The size of the nonlinearity can be measured by taking the difference between the average of the responses to the opposite polarity SST anomalies in an experiment and CONTROL. When this test is performed, it is found that the nonlinearity is small, with the rms magnitude of the 20°–90°N height nonlinearity of order 2 m, and the rms magnitude of the 20°S–20°N precipitation nonlinearity order 0.3 mm day^{-1} in each of the experiments.

The above diagnoses demonstrate that the height and precipitation responses to the imposed SST anomalies are quasi-linear in the idealized experiments. However, the superpositions in Fig. 7 are sufficiently different from the corresponding panels in Fig. 5 so that some of the conclusions drawn from Fig. 5 would be changed if they were to be drawn from Fig. 7, especially with regard to the roles of responses to tropical Atlantic and extratropical forcing. The quasi-linear behavior for the height anomalies contrasts with that reported by Yin and Battisti (2001), who found a nonlocal and nonlinear response in a conceptually similar set of idealized experiments.

2) WAVE PROPAGATION

The most straightforward mechanism for explaining the midlatitude equilibrium response to tropical SST anomalies is Rossby wave propagation forced by convective heating anomalies that develop locally in response to the SST anomalies (early studies of this mechanism include Egger 1977; Opsteegh and Van den Dool 1980; Hoskins and Karoly 1981). Jin and Hoskins (1995) show that upper-tropospheric meridional wind perturbations provide a useful diagnostic for tracing the origins and regions of influence of these waves.

Figure 8 shows the 200-hPa meridional wind response from the idealized experiments. The GLOBE and TROPICS responses (Figs. 8a and 8b) are not easily interpretable; however, the responses to the regional SST anomalies are more easily related to responses expected from simpler diagnostic models. As might be expected from the linearity of the 500-hPa height response, the responses shown in Fig. 8 can be recovered from superposition of the various other 200-hPa meridional wind responses, and the GLOBE response can be understood as the sum of the responses from the various regional SST anomalies. The INDOPAC response (Fig. 8d) clearly shows wave trains in both hemispheres originating in the Indian Ocean/western Pacific sector, arcing across the Pacific, and returning to the equator again near the forcing region. The pattern in the North Pacific/North American region is in phase with the Jin and Hoskins (1995) response to heating at 60°E with a 3D DFJ background state (their Fig. 16c). The pattern is also similar in structure and wavelength, although with a phase difference, to the pattern obtained by Jin and Hoskins forced by heating centered on the equator and 180°. The Jin and Hoskins calculation includes wave–mean flow interaction (e.g., Simmons et al. 1983), but eliminates transient eddy forcing of the stationary waves. Comparing the heating anomaly and response in INDOPAC to the responses found by Jin and Hoskins to heating at 60°E and 180°, a preliminary interpretation is that the wave train in the Northern Hemisphere results from interference between the responses to the positive heating anomalies in the western Pacific and the Indian Ocean, with the Indian Ocean forcing dominating. A similar interpretation results by analogy with the results of Ting and Sardeshmukh (1993) who, using a stationary wave model linearized about a DJF observed climatological basic state, find a nodal line in the sensitivity to tropical forcing near 120°E. According to the Ting and Sardeshmukh linear model result, the atmospheric response to positive forcing to the west of this nodal line will interfere destructively with the response to positive forcing to the east.

Wave trains can also be seen in TROPATL (Fig. 8f), originating in the equatorial Atlantic. However, as opposed to the wave trains in INDOPAC, the wave train in TROPATL is confined primarily to the Southern Hemisphere. The lack of midlatitude Northern Hemisphere response in TROPATL and the prominence of the Southern Hemisphere midlatitude wave train could be due to upper-tropospheric climatological easterlies over near-equatorial South America producing an evanescent response in the Northern Hemisphere to TROPATL heating anomalies (Fig. 6f) located primarily in the Southern Hemisphere, (the mechanism of Webster and Holton 1982). Other possible explanations are the structure of the Rossby wave source produced by the divergent outflow from the heating anomalies (Sardeshmukh and Hoskins 1988), or the refraction properties of the 3D background flow.

In EASTPAC (Fig. 8e), the Northern Hemisphere midlatitude wave train also appears to originate in the western Pacific, but to intensify in the eastern Pacific. These characteristics probably result from the combination of influences from central Pacific and eastern Pacific precipitation anomalies (Fig. 6e). In EXTRATROPICS (Fig. 8c), there appear to be an equatorward propagating wave trains originating over the North Pacific and North Atlantic. There are no obvious tropical sources for this wave train.

b. Zonal mean winds and the unforced variability of the trend

We examine the simulated and observed zonal mean trends in this section. There are several reasons to do

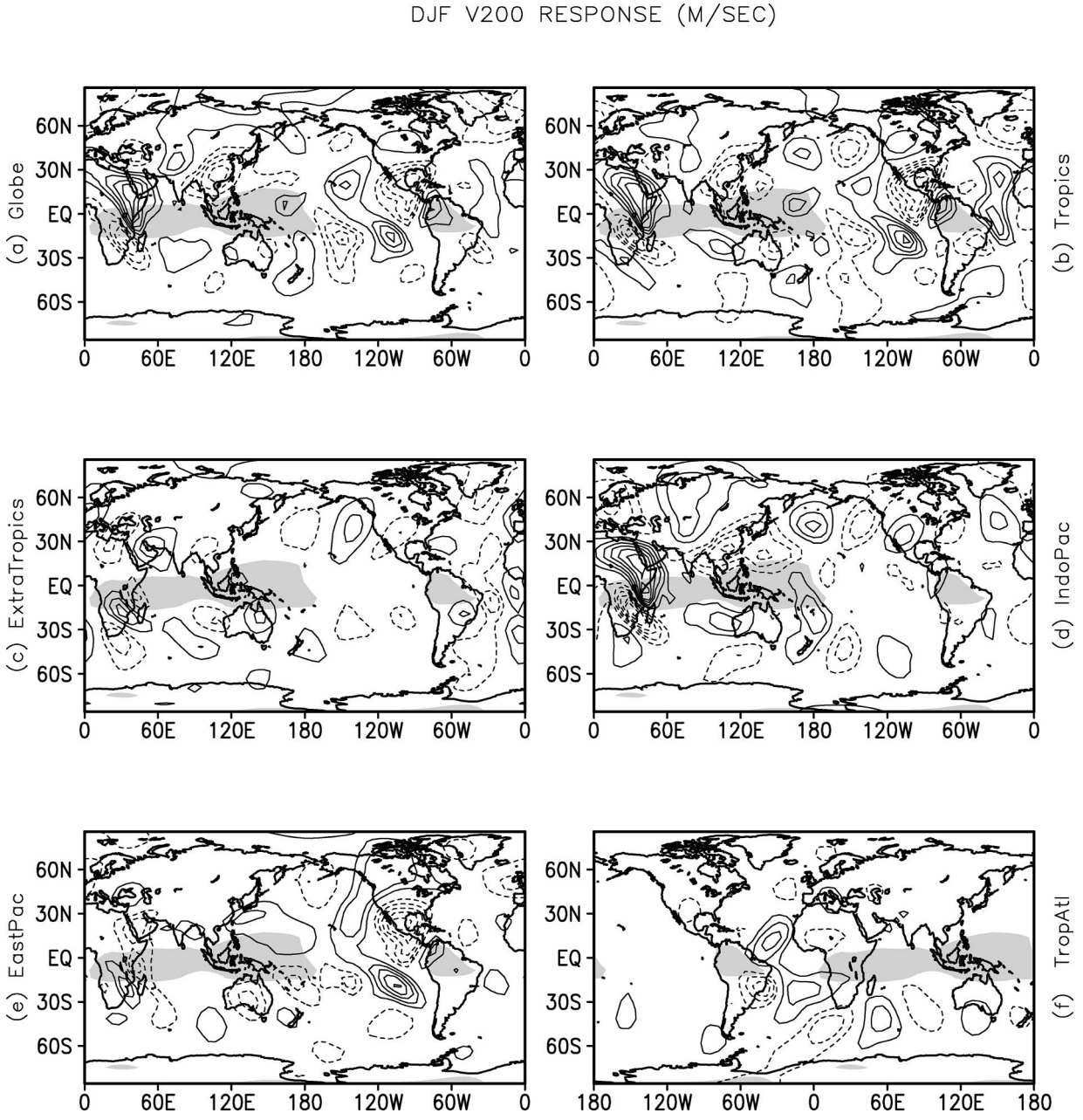

FIG. 8. The response of the 200-hPa meridional wind for (a) GLOBE, (b) TROPICS, (c) EXTRATROPICS, (d) INDOPAC, (e) EASTPAC, and (f) TROPATL (rotated 180° longitude from other panels). The contour interval is 0.5 m s^{-1} except in (c) where is it 0.3 m s^{-1} and the zero contour is not shown. The regions of tropical easterlies in the 200-hPa zonal wind of CONTROL are shaded.

this. First, the observed trend shown in Fig. 1a has a strong projection on the zonal mean. Additionally, from an interpretive viewpoint, many characteristics of the steady-state two-dimensional tropospheric zonal mean flow and mass field can be inferred from the one-dimensional upper-tropospheric/lower-stratospheric zonal mean zonal and meridional velocities, and also the mechanisms that force zonal means are simpler to describe and infer than those for three-dimensional fields.

The observed and simulated trends of the DJF 200-mb zonal mean zonal and meridional winds, u_{200} and v_{200}, are shown in Fig. 9. Surface trends in the u fields are essentially of the same sign as those shown in Fig. 9, but of smaller magnitude, and the surface v trends are of the opposite sign from those shown in Fig. 9, as would be expected of overturning cells extending through the troposphere. Note that errors could be large in the observed trends for u_{200} and v_{200} in the SH and the Tropics, and for v_{200} in the NH extratropics.

The timescales are sufficiently long so that it is ap-

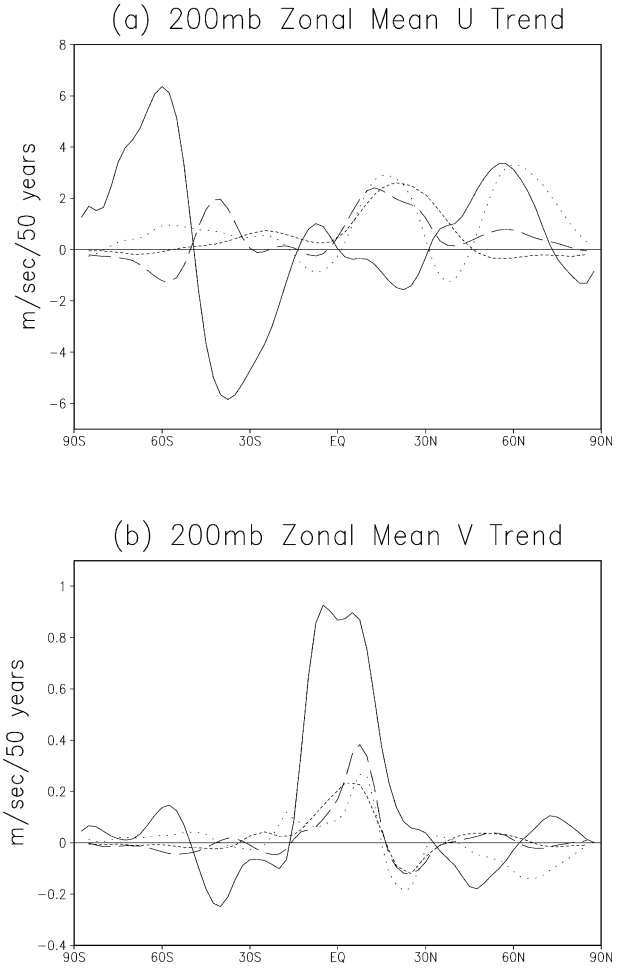

FIG. 9. The 200-mb DJF trends for zonal means of (a) zonal wind and (b) meridional wind. The solid curves are for the NCEP–NCAR reanalysis, long dash for the T63 ensemble, short dash for the T21 ensemble, and dotted for the member of the T63 ensemble shown in Fig. 1d.

propriate to use arguments based on the theory of steady-state balance to understand the processes important in the trends. Trends can be inferred from differences in steady states (cf. the motivation for the idealized experiments given in section 4a). As discussed in the appendix, there are distinctive differences between the responses to thermal and mechanical forcing that can be used for diagnostic purposes. An argument is given there that suggests the response to mechanical forcing should have a negative correlation between the upper tropospheric zonal and meridional winds, with positive zonal mean zonal winds in the region of the forcing, while the meridional circulation response to midlatitude thermal forcing should be much less apparent and probably have the opposite correlation.

Figure 9 shows that the NH extratropical upper-tropospheric zonal and meridional winds are anticorrelated in the reanalysis, from 30°–60°N and poleward of 70°N, which indicates that the dominant forcing of the observed trend of the zonal winds in the NH extratropics is mechanical. From the argument of Held (1975) and Eq. (A11) in the appendix, the observed positive u_{200} trend in NH midlatitudes can probably be explained by an increasing trend in mechanical stirring in that latitude band. Zonal mean trends in the reanalysis also indicate that mechanical forcing is important in low latitudes, but compensated by thermal forcing; however, the accuracy of the mean meridional wind trend in particular might be suspect in that region. In the model ensemble means, on the other hand, the 200-hPa zonal mean zonal wind and meridional wind trends are positively correlated between the equator and 15°N, and negatively correlated from 15°N to about 30°N latitudes. Poleward of 30°N, both the zonal and meridional wind trends are small. It can be inferred that in the ensemble means, thermal forcing dominates the zonal wind trends at low latitudes, and mechanical forcing dominates between 20° and 30°N, while at higher latitudes mechanical forcing and thermal forcing are both weak.

Examination of the trends of the individual members of the model ensembles gives an entirely different picture in the extratropical NH, and one that much more closely resembles the reanalysis. The individual members have u_{200} trends that can be comparable in magnitude with those in the reanalysis, and that show the out of phase relationship with the respective v_{200} trends characteristic of the response to midlatitude mechanical stirring. The u_{200} and v_{200} trends for the case of Fig. 1d are shown in Fig. 9 and illustrate this point. The u_{200} trend for this case has about the same magnitude as the observed trend near 60°N, although a different meridional structure, while the v_{200} trend for this case is anticorrelated as would be expected for mechanical forcing. In the Tropics, however, the ensemble mean and the single case trends are not distinguishable, and both indicate dominant thermal forcing.

The model simulations demonstrate that large higher latitude zonal mean variability could occur in the atmosphere even on multidecadal timescales without variation in the external forcing. This variability is primarily mechanically forced in the model, and observed trends in the NH midlatitudes appear to have similar properties to the internally generated variability in the model simulations. The features found in the model, internal variability of the zonal mean generated by variability of midlatitude stirring, are similar to the well-known properties of the higher frequency ''index cycle'' zonal mean variability (summarized for example by Robinson 1996). However, it is beyond the scope of this paper to examine the sources of variability of the stirring in the simulations.

Although mechanically forced variability in the intraensemble model trend is not related to variability in the tropical thermal forcing, the same conclusion cannot be made for the observed trend. Even given that the midlatitude observed trends are mechanically forced, this type of response could result from displacements

of the storm tracks initiated by the tropical thermal forcing.

7. Discussion and conclusions

Ensemble simulations of the atmospheric response to trends in SST over the past half century have been made using the COLA AGCM in order to help understand the mechanisms of the observed trend in the DJF NH 500-hPa height. The results, which are summarized below, are suggestive but not conclusive concerning the causes of the observed trends, and seem to indicate potentially important roles for both internal variability and tropical forcing for trends in the North Atlantic.

There is a clearly defined pattern in the response of the ensemble mean of the AGCM 500-hPa DJF height to the SST trends, which does not appear to depend strongly on model horizontal resolution. This pattern has only a moderate resemblance to the structure of the observed height trend, and this resemblance is mostly in features in the eastern Pacific. The COLA model's estimate of the forced component of the trend is very similar to the estimate of Thompson et al. (2000) of the part of the observed trend that cannot be explained by the AO. We also note that the structure of the COLA model's forced response is close to the response to projected GHG found by Fyfe et al. (1999).

However, there is also substantial variability of the trends between the ensemble members with a structure strongly resembling the AO. This variability has large enough magnitude and the general structural features (although possibly distorted due to systematic errors in the model) to explain the difference between the forced response and the observed trend. The magnitude of the observed trend is toward the upper end of the model's internal variability. If the model behavior is realistic, then much of the AO-like part of the observed trend could be noise produced by internal atmospheric variability unrelated to the SST forcing, and inherently unpredictable. Apparently by chance, the forced component of the trend has a spatial structure that is not similar to the AO, so that the two components can be easily distinguished. However, the result that internal atmospheric dynamics can produce such a large magnitude of AO variability on the multidecadal timescale in the model seems to be at odds with Feldstein (2002), who concluded that the observed trend in the AO cannot be explained by the observed internal variability. This aspect of the results needs to be better understood before the model-based interpretation can be accepted as valid and applicable to understanding the observed trends.

On the other hand, the forced response of the COLA model does not reproduce some of the results found by Hoerling et al. (2001) with CCM, particularly the AO-like structure in the North Atlantic. This indicates that the results are model dependent. The results obtained with the COLA model also do not appear to agree with those found by Shindell et al. (1999), who attribute the AO-like structure of the observed trend to effects of changing GHG on the stratospheric circulation. However, the COLA model has poor stratospheric resolution, and the ensembles were conducted with constant GHG, and consequently do not include the GHG stratospheric effect (or the effect of changing GHG on the land surface energy budget). Future experiments planned as part of the C20C project should help isolate the role of the stratospheric/GHG mechanism.

Idealized experiments were carried out to understand the forced response, and further diagnostic analysis was performed to infer information about the mechanisms behind AO-related trends in the zonal mean winds. The idealized experiments were simulations with constant-in-time SST anomalies, which had the structure of the observed SST trend. The idealized experiments produced a quasi-linear NH DJF 500-hPa height response to the imposed SST anomalies and identified the Indian Ocean/western Pacific and eastern Pacific as the dominant forcing regions, and showed little response in the North Atlantic to extratropical or tropical Atlantic SST anomalies. Tropical SST anomalies appear to force Rossby wave trains that follow paths strongly dependent on the location of the forcing relative to the climatological stationary waves.

A diagnosis of the trends of the upper-tropospheric zonal mean winds was carried out. The source of the intraensemble variability in the trend of the zonal mean zonal wind (closely related to the AO variability) and the source of the trend in the observed zonal mean zonal wind were inferred to be trends in midlatitude stirring by transient eddies. In the model, these stirring trends were not related to tropical forcing; however, this conclusion cannot be made for the observations.

Acknowledgments. This research was supported by grants from the National Science Foundation (ATM 98-14295, ATM 99-07915), the National Oceanic and Atmospheric Administration (NA 96-GP0056), the National Aeronautics and Space Administration (NAG 5-8202), and the Office of Science (BER), U. S. Department of Energy (DE-FG02-01ER63256). We thank three anonymous reviewers for their careful and skeptical reading of the manuscript.

APPENDIX

Equilibrium Zonal Mean Response to Transient Forcing

It can be seen in Schneider (1984) that the characteristic steady upper-tropospheric tropical zonal mean response to a deep heat source near the equator is positive/negative zonal winds associated with poleward/equatorward meridional winds (positive/negative correlation of the zonal mean zonal and meridional winds in the NH/SH). On the other hand, the characteristic tropical and midlatitude response to horizontal eddy mo-

mentum flux forcing has the opposite sign correlation between the zonal and meridional winds, with positive/negative zonal wind associated with equatorward/poleward meridional wind in the NH upper troposphere. This suggests that there are distinctive differences between the responses to thermal and mechanical forcing that can be used for diagnostic purposes.

DeWeaver and Nigam (2000) also note that in the NCEP–NCAR reanalysis (Kalnay et al. 1996), the responses of both the column mean and surface monthly mean zonal mean zonal winds to forcing by eddy momentum flux divergences are proportional to the column mean forcing. They note that this relationship between the zonal winds, especially in the upper troposphere, and the forcing is not well understood.

It is shown below that pure mechanical and pure thermal forcing should have different signatures in the upper-tropospheric zonal mean winds. In the Northern Hemisphere midlatitudes, mechanical forcing will produce zonal and meridional winds that are negatively correlated, while thermal forcing will produce a meridional wind response that is negligible or positively correlated with the zonal wind response. The result also provides a basis for the relationship found by DeWeaver and Nigam (2000).

Consider the zonal mean Boussinesq quasigeostrophic thermal wind, zonal momentum, heat, and continuity equations:

$$f_0\frac{\partial u}{\partial z} = -\frac{g}{a\Theta}\frac{\partial \theta}{\partial y}, \tag{A1}$$

$$f_0 v = \frac{1}{a}\frac{\partial}{\partial y}(\overline{u'v'}) + \frac{\partial F_x}{\partial z}, \tag{A2}$$

$$w\frac{d\theta_0}{dz} = -\frac{1}{a}\frac{\partial}{\partial y}(\overline{v'\theta'}) + \frac{\theta_e - \theta}{\tau} - \frac{\partial F_\theta}{\partial z}, \tag{A3}$$

$$\frac{1}{a}\frac{\partial v}{\partial y} + \frac{\partial w}{\partial z} = 0, \tag{A4}$$

where the zonal mean variables are the zonal, meridional, and vertical velocities u, v, and w, respectively, and the potential temperature is θ. The coordinates are height z in the vertical, measured upward from the ground, and distance ay in the meridional direction, where y is dimensionless and a is the earth's radius. The Coriolis force f_0 is a constant appropriate for middle latitudes. Forcing includes the zonally averaged horizontal eddy momentum and heat fluxes, $\overline{u'v'}$ and $\overline{v'\theta'}$, radiative/convective heating parameterized as relaxation to specified θ_e with time constant τ, and zonal momentum and temperature fluxes due to small-scale turbulent mixing F_x and F_θ. Other parameters are gravity g, typical stratification $d\theta_0/dz$, and typical temperature Θ.

Upper boundary conditions are taken to be $w(H) = F_x(H) = F_\theta(H) = 0$, and surface boundary conditions are $w(0) = 0$, $F_x(0) = -c_m|v_s|u$, and $F_\theta(0) = c_h|v_s|(\theta_s - \theta)$. The specified parameters are dimensionless drag coefficients for momentum and heat c_m and c_h, and typical surface wind speed v_s. DeWeaver and Nigam (2000) point out the complications of interpretation introduced when these parameters are allowed to be functions of the flow field.

An equation relating the upper-tropospheric zonal wind, the vertically averaged temperature, and the vertically integrated eddy momentum flux is derived by integrating (A1) from $z = 0$ to an upper-tropospheric level H where $w = 0$, as in Held and Hou (1980). Denoting a vertical mean from 0 to H by [ ], $u(0)$ is found from vertical integration of (A2), using $[v] = 0$ from (A4) to be

$$u(0) = -\frac{H}{c_m|v_s|a}\frac{d}{dy}[\overline{u'v'}],$$

so that

$$u(H) = -\frac{gH}{f_0 a\Theta}\frac{d[\theta]}{dy} - \frac{H}{c_m|v_s|a}\frac{d}{dy}[\overline{u'v'}]. \tag{A5}$$

An equation for $[\theta]$ is derived by taking the vertical mean of (A3), assuming that $F_\theta(0)$ can be ignored relative to the other terms, and rearranging, so that

$$[\theta] = [\theta_e] - \tau\frac{d\theta_0}{dz}[w] - \frac{\tau}{a}\frac{d}{dy}[\overline{v'\theta'}]. \tag{A6}$$

The continuity equation (A4) is used to find $[w]$:

$$[w] = \frac{H}{a}\frac{dV}{dy}, \tag{A7}$$

where

$$V = \frac{1}{H^2}\int_0^H \left(\int_z^H v\, dz'\right) dz. \tag{A8}$$

Substitution of $[\theta]$ from (A6) into (A5), using (A8) gives

$$u(H) = u_e(H) + \frac{\tau gH}{f_0 a^2\Theta}\left(H\frac{d\theta_0}{dz}\frac{d^2V}{dy^2} + \frac{d^2}{dy^2}[\overline{v'\theta'}]\right) - \frac{H}{c_m|v_s|a}\frac{d}{dy}[\overline{u'v'}], \tag{A9}$$

where

$$u_e(H) = -\frac{gH}{f_0 a\Theta}\frac{d[\theta_e]}{dy}.$$

Using (A2) and (A8) with the definition $\overline{U'V'} = (1/H^2)\int_0^H(\int_z^H \overline{u'v'}\, dz')\, dz$, gives $V = (1/f_0 a)(d/dy)(\overline{U'V'}) - (1/f_0 H)[F_x]$, and assuming F_x is small except in a thin surface boundary layer leads to

$$V = \frac{1}{f_0 a}\frac{d}{dy}(\overline{U'V'}). \tag{A10}$$

Finally, (A10) is substituted into (A9), giving

$$u(H) = u_e(H) + \frac{\tau g H}{f_0 a^2 \Theta}\left(\frac{H}{f_0 a}\frac{d\theta_0}{dz}\frac{d^3\overline{U'V'}}{dy^3} + \frac{d^2}{dy^2}[\overline{v'\theta'}]\right) - \frac{H}{c_m|v_s|a}\frac{d}{dy}[\overline{u'v'}]. \quad \text{(A11)}$$

Equation (A11) is closely related to the transformed Eulerian mean (TEM) Eliassen–Palm (EP) flux formalism of Edmon et al. (1980). The bracketed term on the rhs of (A11) multiplied by τ is proportional to $d[w^*]/dy$, where w^* is the TEM vertical velocity in a steady state with $F = 0$. The eddy fluxes are quasi noninteracting when $d^3\overline{U'V'}/dy^3 + [f_0 a/H(d\theta_0/dz)]\,(d^2/dy^2)\,[\overline{v'\theta'}] = 0$, a sufficient condition for which is zero EP flux, although, as can be seen from (A11), true noninteraction requires the vertically integrated eddy momentum flux to be zero as well.

Using Δ to denote a change, the case of pure mechanical forcing is the response to $\Delta\overline{u'v'} \neq 0$, with no change in the thermal forcing, $\Delta\theta_e = \Delta\overline{v'\theta'} = 0$. A typical situation relevant to tropospheric structure is one where $\Delta\overline{u'v'}$ has an upper-tropospheric midlatitude maximum, with small values near the ground and in the stratosphere. Taking $\Delta\overline{u'v'} = (z/H)\Delta\overline{u'v'}(H)$ for the purposes of estimation gives $\Delta\overline{U'V'} = \Delta\overline{u'v'}(H)/3$, $\Delta[\overline{u'v'}] = \Delta\overline{u'v'}(H)/2$, and $\Delta V = \Delta v(H)/3$. Taking $(d^2/dy^2)\Delta\overline{U'V'} \propto -\Delta\overline{U'V'}$, (A11) implies that the relationship between mechanically forced changes in the zonal and meridional upper tropospheric velocities is $\Delta u(H) \propto -(d/dy)\Delta\overline{u'v'}(H) \propto -\Delta v(H)$. The surface perturbation zonal wind is of the same sign as $\Delta u(H)$ in this case.

It has also been established zonally asymmetric mechanical stirring produces zonal mean flow acceleration ($\partial\overline{u'v'}/\partial y < 0$) in the latitudes of stirring and zonal mean deceleration ($\partial\overline{u'v'}/\partial y > 0$) in adjacent regions of wave dissipation due to the properties of the Rossby waves (stationary or transient) forced by the stirring (Held 1975). Then using (A11), the mechanically forced $u(H) > 0$ in the latitudes of stirring and $u(H) < 0$ in latitudes where the mechanically forced disturbances dissipate.

For the case of pure thermal forcing, due to $\Delta\theta_e \neq 0$ or $\Delta\overline{v'\theta'} \neq 0$ with $\Delta\overline{u'v'} = 0$, there is a zonal wind response, but from (A2), $\Delta v(H) = 0$ and there is no meridional wind response to this order of approximation. However, it is expected on energetic grounds that if the meridional circulation response is nonzero, the thermally forced response should have a positive correlation between $u(H)$ and $v(H)$ (although circulation cells that straddle the equator can behave differently). The thermally direct (kinetic energy dissipating) response will reduce and smooth out, but not eliminate completely, the meridional temperature contrasts that would exist in the absence of a meridional circulation response [e.g., that given from (A6) with $[w] = 0$]. Without a meridional circulation response, a heat source in the Northern Hemisphere will produce a maximum temperature response at the latitude of the heating, and positive (negative) $u(H)$ to the north (south) through the thermal wind relation. The kinetic energy producing meridional circulation response will have rising at the latitude of the heating and sinking on the flanks, connected by northward (southward) $v(H)$ to the north (south): that is, a positive correlation between $u(H)$ and $v(H)$.

In the case of mixed thermal and mechanical forcing, there can be compensation with regard to changes in $u(H)$ between the changes in the eddy momentum and changes in the heating. The signature of compensating forcing is small $u(H)$ but large $v(H)$ such as seen in Fig. 9 for the reanalysis near the equator (although the observed relationship is uncertain due to potentially large errors in the data).

In this derivation, the temperature equation (A3), and in particular the parameterized Newtonian cooling, plays a crucial role in the mediating between the structure of the meridional and zonal wind responses. The meridional circulation and surface zonal wind are produced directly by the mechanical forcing, independent from (A3). The temperature response results from a balance between heat advection by this meridional circulation and the parameterized heat sources and sinks. The upper-tropospheric zonal wind response results from thermal wind balance with the temperature response added to the surface zonal wind response. The surface zonal wind responds proportionally to the column mean momentum flux forcing, while the upper-tropospheric zonal wind responds proportionally to a quantity that is related to the column mean momentum flux forcing, at least when this forcing has a simple vertical structure.

REFERENCES

Bretherton, C. S., and D. S. Battisti, 2000: An interpretation of the results from atmospheric general circulation models forced by the time history of the observed sea surface temperature distribution. *Geophys. Res. Lett.*, **27,** 767–770.

DeWeaver, E., and S. Nigam, 2000: Do stationary waves drive the zonal-mean jet anomalies of the northern winter? *J. Climate,* **13,** 2160–2176.

Edmon, H. J., Jr., B. J. Hoskins, and M. E. McIntyre, 1980: Eliassen-Palm cross sections for the troposphere. *J. Atmos. Sci.,* **37,** 2600–2616.

Egger, J., 1977: On the linear theory of the atmospheric response to sea surface temperature anomalies. *J. Atmos. Sci.,* **34,** 603–614.

Feldstein, S. B., 2002: The recent trend and variance increase of the annular mode. *J. Climate,* **15,** 88–94.

Folland, C., J. Shukla, J. Kinter, and M. Rodwell, 2002: The Climate of the Twentieth Century Project. *CLIVAR Exchanges,* **7,** 37–39. [Available from International CLIVAR Project Office, Southampton Oceanography Centre, Empress Dock, Southampton, SO14 3ZH, United Kingdom; also available online at http://www.clivar.org/publications/exchanges/ex24/ex24.pdf]

Fyfe, J. C., G. J. Boer, and G. M. Flato, 1999: The Arctic and Antarctic Oscillations and their projected changes under global warming. *Geophys. Res. Letters,* **26,** 1601–1604.

Gill, A. E., 1980: Some simple solutions for heat-induced tropical circulations. *Quart. J. Roy. Meteor. Soc.,* **106,** 447–462.

Held, I. M., 1975: Momentum transport by quasi-geostrophic eddies. *J. Atmos. Sci.,* **32,** 1494–1497.

——, and A. Y. Hou, 1980: Nonlinear axially symmetric circulations in a nearly inviscid atmosphere. *J. Atmos. Sci.,* **37,** 515–533.
Hoerling, M. P., J. W. Hurrell, and T. Xu, 2001: Tropical origins for recent North Atlantic climate change. *Science,* **292,** 90–92.
Hoskins, B. J., and D. J. Karoly, 1981: The steady linear response of a spherical atmosphere to thermal and orographic forcing. *J. Atmos. Sci.,* **38,** 1179–1196.
Hulme, M., 1994: Validation of large-scale precipitation fields in general circulation models. *Global Precipitation and Climate Change,* M. Desbois and F. Desalmand, Eds., NATO ASI Series I, Vol. 26, Springer-Verlag, 387–406.
Jin, F. F., and B. J. Hoskins, 1995: The direct response to tropical heating in a baroclinic atmosphere. *J. Atmos. Sci.,* **52,** 307–319.
Kalnay, E., and Coauthors, 1996: The NCEP/NCAR 40-Year Reanalysis Project. *Bull Amer. Meteor. Soc.,* **77,** 437–471.
Kinter, J. L., III, M. J. Fennessy, V. Krishnamurthy, and L. Marx, 2002: On apparent decadal shifts in tropical atmospheric circulation in reanalysis. COLA Rep. 122, 20 pp. [Available from COLA, 4041 Powder Mill Rd., Suite 302, Calverton, MD 20705.]
Magnusdottir, G., 2001: The modeled response of the mean winter circulation to zonally averaged SST trends. *J. Climate,* **14,** 4166–4190.
——, and R. Saravanan, 1999: The response of atmospheric heat transport to zonally averaged SST trends. *Tellus,* **51A,** 815–832.
Mehta, V. M., M. J. Suarez, J. V. Manganello, and T. L. Delworth, 2000: Oceanic influence on the North Atlantic Oscillation and associated Northern Hemisphere climate variations: 1959–1993. *Geophys. Res. Lett.,* **27,** 121–124.
Opsteegh, J. D., and H. M. Van den Dool, 1980: Seasonal differences in the stationary response of a linearized primitive equation model: Prospects for long range weather forecasting? *J. Atmos. Sci.,* **37,** 2169–2185.
Robertson, A. W., C. R. Mechoso, and Y.-J. Kim, 2000: The influence of Atlantic sea surface temperature anomalies on the North Atlantic Oscillation. *J. Climate,* **13,** 122–138.
Robinson, W. A., 1996: Does eddy feedback sustain variability in the zonal index? *J. Atmos. Sci.,* **53,** 3556–3569.
Rodwell, M. J., D. P. Rowell, and C. K. Folland, 1999: Oceanic forcing of the wintertime North Atlantic Oscillation and European climate. *Nature,* **398,** 320–324.
Sardeshmukh, P. D., and B. J. Hoskins, 1988: The generation of global rotational flow by steady idealized tropical divergence. *J. Atmos. Sci.,* **45,** 1228–1251.
Schneider, E. K., 1984: Response of the annual and zonal mean winds and temperatures to variation in the heat and momentum sources. *J. Atmos. Sci.,* **41,** 1093–1115.
——, 2002: The causes of differences between equatorial Pacific SST simulations of two coupled ocean–atmosphere general circulation models. *J. Climate,* **15,** 449–469.
Shindell, D. T., R. L. Miller, G. A. Schmidt, and L. Pandolfo, 1999: Simulation of recent northern winter climate trends by greenhouse-gas forcing. *Nature,* **399,** 452–455.
Simmons, A. J., J. M. Wallace, and G. W. Branstator, 1983: Barotropic wave propagation and instability, and atmospheric teleconnection patterns. *J. Atmos. Sci.,* **40,** 1363–1392.
Thompson, D. W. J., J. M. Wallace, and G. C. Hegerl, 2000: Annular modes in the extratropical circulation. Part II: Trends. *J. Climate,* **13,** 1018–1036.
Ting, M., and P. D. Sardeshmukh, 1993: Factors determining the extratropical response to equatorial diabatic heating anomalies. *J. Atmos. Sci.,* **50,** 907–918.
Trenberth, K. E., and C. J. Guillemot, 1998: Evaluation of the atmospheric moisture and hydrological cycle in the NCEP/NCAR reanalyses. *Climate Dyn.,* **14,** 213–231.
Wallace, J. M., and D. W. J. Thompson, 2002: Annular modes and climate prediction. *Phys. Today,* **55,** 28–33.
Webster, P. J., and J. R. Holton, 1982: Cross-equatorial response to middle latitude forcing in a zonally varying basic state. *J. Atmos. Sci.,* **39,** 722–733.
Yin, J. H., and D. S. Battisti, 2001: The importance of tropical sea surface temperature patterns in simulations of Last Glacial Maximum climate. *J. Climate,* **14,** 565–581.